Article

Comparison of the fluidized state stability from Radioactive Particle Tracking results applied

Gabriel Salierno[1,2,*], Anton Gradišek[3], Mauricio Maestri[2], Julia Picabea[2], Miryan Cassanello[2], Cataldo De Blasio[1], María Angélica Cardona[4], Daniel Hojman[4], Héctor Somacal[4]

[1] Faculty of Science and Engineering, Energy Technology, Åbo Akademi University. Vaasa, Finland; cataldo.deblasio@abo.fi

[2] Laboratorio de Reactores y Sistemas para la Industria–LARSI, Dep. Industrias, FCEyN, Universidad de Buenos Aires, Int. Güiraldes 2620, C1428BGA Buenos Aires, Argentina; miryan@di.fcen.uba.ar

[3] Department of Intelligent Systems, Jožef Stefan Institute, Ljubljana, Slovenia; anton.gradisek@ijs.si

[4] Laboratorio de Diagnóstico por Radiaciones–LaDiR, Dep. Física Experimental, Comisión Nacional de Energía Atómica (CNEA), San Martín, Buenos Aires, Argentina; hojman@tandar.cnea.gov.ar

* Correspondence: gabriel.salierno@gmail.com

Abstract: Currently, various industrial processes are carried out in fluidized bed reactors, such as fermentation, water treatment, and algae growth. Knowing its internal dynamics is fundamental for the intensification of these processes. This work assesses the motion of fluidized calcium alginate spheres under the influence of an upward fluid flow within a 1.2 m high and 0.1 m inner diameter acrylic column. The Radioactive Particle Tracking technique is a proper methodology to study the internal dynamics of these kinds of equipment. Liquid-Solid Fluidized Bed is compared with the Gas-Liquid-Solid Fluidized Bed operation mode in terms of mixing behavior. Data gathered is analyzed in view of Shannon entropy as a dynamic mixing measure. Mixing times are found to be of the same order of magnitude. However, the Liquid-Solid Fluidized Bed achieves a lower homogenization degree. Also, we found good agreement between two criteria for assessing stability for the mixed state: the Shannon Entropy time-series plateau and the Glansdorff-Prigogine criterion based on Fisher information.

Keywords: Fluidization; Radioactive Particle Tracking; Information Geometry; Stability Criteria

1. Introduction

Fluidization has a long history of utility for mineral sorting and has been used for the purpose already for several hundreds of years [1]. Many catalytic processes and operations in the chemical industry are currently carried out in fluidized beds. The use of expanded beds allows a better homogenization of cell culture media. Methodologies such as adsorption or fluidized bed chromatography are currently being established [2,3], which have had promising results in the extraction of biological products of industrial interest, given the reduction of the operating volume, which is the objective of process intensification [4–6]. Their underlying dynamics are fundamental for the proper design of the units and implementing process intensification strategies [7,8]. Such dynamics are governed by body forces (gravity, buoyancy) and external friction forces. From the microscopic contribution of each fluid element and the particles of the system emerge observables such as bed height, pressure drop, distribution of shear forces, mixing times, and turbulent kinetic energy. The correct prediction of these observables depends upon the precision with which these macroscopic forces are described and remains an open problem to a large extent [9,10]. On the other hand, in the last decades, experimental methods have been developed to determine trajectories of particles in free movement within multiphase equipment. The

Radioactive Particle Tracking (RPT) technique involves determining the trajectory of a single radioactive tracer representing the solid particles of the system, providing comprehensive information on multiphase flows [11–15]

Shannon (or information) entropy is a statistic that estimates the homogeneity of a probability distribution which can be used as a mixing index [16,17]. The Shannon entropy is a property of any probability distribution, $\{p_i\}, i \in (1; ...; N)$ where N is the number of bins into which the valid range of the distribution is divided. If N is finite, the discrete probability density function is often called probability simplex. In the context of RPT, the valid range of the probability distribution will be enclosed within the space that the tracer trajectory reaches, and the bins will result from the granularity with which that space is divided. The Shannon entropy is useful to quantify the mixing of solid particles in suspension or liquid elements from RPT data [12].

Alginates form a hydrogel in aqueous calcium solutions, which are traditionally used to immobilize enzymes and microorganisms [18]. Its potential use as a contaminant adsorbent [19] and support for inorganic catalysts are also currently being explored [20,21]. This work compares the mixing behavior and the pseudo stationary state stability of fluidized bed columns. The motion of 5 mm calcium alginate gel spheres suspended within liquid-solid and gas-liquid-solid turbulent media is examined with RPT. Information theory is applied to study particle mixing, and information geometry is employed to assess the stability of the mixed state.

2. Materials and Methods

2.1 - The Radioactive Particle Tracking technique

The method of tracking a single radioactive particle (Radioactive Particle Tracking - RPT) consists of simultaneously counting the number of gamma rays that arrive from a stable tracer in motion to a set of high-energy radiation detectors strategically located around the equipment under study. The number of photons that interact with each detector is proportional to the solid angle subtended by the detector to the radioactive source used as a tracer, which in turn depends on the tracer-detector distance [14]. Therefore, the simultaneous detection of radiation with a set of detectors arranged around the column makes it possible to determine the mean position of the tracer at each sampling period.

The RPT technique is based on considering an isotropic gamma emission pattern. Negative-beta decay provides such gamma emission. This emission mechanism is characteristic of neutron-rich nuclei. Also, following the ALARA safety philosophy, the tracer must be properly active during the experiments. It is also convenient that it has not so long a half-life to reach a stable state after being used quickly. ^{198}Au (Eγ = 0.412 MeV; $t_{1/2}$ = 2.7 d) is thus a good chosen option. The tracer consists of a 1mm diameter high-density polyethylene (PEAD) hollow sphere that seals a fragment of a few gold micrograms inside [22]. The gamma sources are obtained by neutron bombardment in the RA1 nuclear reactor of the National Atomic Energy Commission (CNEA – Buenos Aires - Argentina). The resulting radioactivity depends upon the exposure time and on the neutron flux. The tracer path

is followed for several hours with a sampling period of 30ms. For the reconstruction, a calibration stage was performed by measuring the counts while locating the tracer at known positions within the system. The signal distribution, the tracer intensity, the media attenuation, and the dead time of the detector system were fitted for each detector to represent their response to radiation. Details of the reconstruction procedure can be found elsewhere [13,14]. Experiments are carried out in an acrylic column (1.2 m height, 0.1 m inner diameter) surrounded by an array of 16 NaI(Tl) 2" scintillation detectors (Figure 1).

Figure 1. Experimental setup: RPT detectors array.

Two modes of fluidization are considered in this work:

- Liquid-Solid Fluidized Bed (LSFB), where the liquid flows upward while the particulate solid phase is in batch mode [23]. In this case, there is no gas flow.

- Gas-Liquid-Solid Fluidized bed (GLSFB), where the liquid and the particulate phase are in batch mode while gas flows upward [12].

2.2 - Liquid-solid fluidized bed (LSFB) operational parameters

In the LSFB, the liquid phase is a solution of CaCl$_2$ 0.05M (ϱ_L = 1008 kg/m³; μ_L = 1.02 mPa.s) in water, flowing in a closed-loop impelled by a centrifugal pump moderated by a diaphragm valve. The liquid superficial velocity (u_L) is set and controlled at different constant values between 0.028 to 0.036 m/s of superficial liquid velocity. The liquid enters into the column from the bottom through a distributor of 2.2% effective section. Gel beads (ϱ_s = 1030 kg/m3) content is about 8% v/v.

2.3 - Gas-Liquid-Solid Fluidized Bed (GLSFB) operational parameters

In the case of a GLSFB, the column is operated with compressed air (ϱ_g = 1.22 kg/m³; μ_g = 18 µPa.s) flowing upwards through a distributor located at the base of the column. The air entered the column through 42 holes of 1 mm, resulting in an effective cross-section of 0.42 %. The superficial velocity of air (u_g) is varied between 0.01 and 0.10 m/s. The condensed phase is an aqueous solution of CaCl$_2$ 0.05M (ϱ_L = 1008 kg/m³; μ_L = 1,02 mPa.s) with 8% v/v of 5 mm diameter calcium alginate spheres (ϱ_s = 1030 kg/m³). The liquid-solid suspension is in batch mode. The room temperature is set at 24°C.

3. Shannon Entropy and Mixing behavior

Shannon entropy [24], or information entropy, is a statistic related to the homogeneity of a probability distribution. If applied to the probability distribution of discrete particle positions [25], which represents suspended solids or liquid elements, it can be used as a mixing index [26]. In this work, we define the statistic $\Omega(t)$ relating the instantaneous entropy of the distribution with the maximum that could be reached for the number of bins or sections considered in the discretization (Eq. 1).

$$\Omega(t) = -\frac{\sum_{i=1}^{N}[p_{i(t)}\ln(p_{i(t)})]}{\ln(N)} \tag{1}$$

Where N is the number of bins in which the simplex has been discretized and $p_{i(t)}$ is the normalized frequency of finding the tracer at the i-th position (with i belonging to the natural numbers between 1 and N). The magnitude $\Omega(t)$ takes real values between 0 and 1 because the Shannon entropy is normalized by the value that corresponds to the maximum possible entropy, uniquely associated with the equiprobable distribution.

To calculate the Shannon entropy, we first construct a manifold of trajectories from a properly long single tracer trajectory obtained by RPT. The tracer is carefully built to mimic the dynamics of the rest of the particles. Then, considering ergodicity, we interpret the manifold as an injection of particles at a given region of the space. Figure 2 shows the axial projection of a trajectory manifold obtained by RPT experiments on the GLSFB.
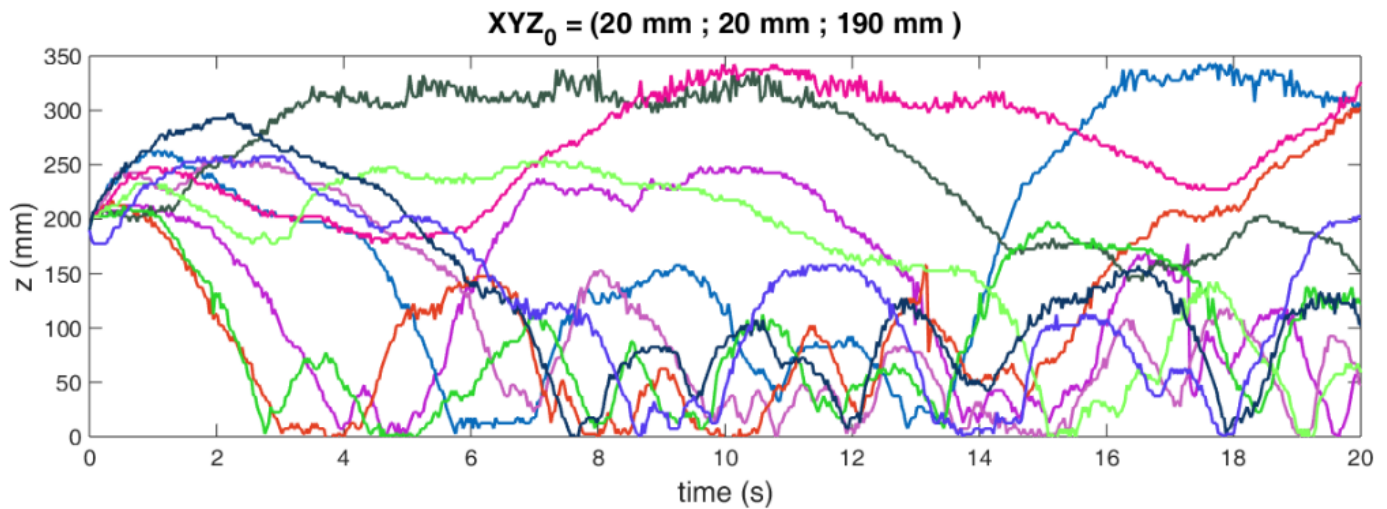
Figure 2. Axial projection of a trajectories manifold, obtained from GLSFB, starting from a specific position.

Figure 3 illustrates how the histogram of positions of particles that begin their trajectory in a portion of the column at a certain height varies over time. The probabilities of visiting different regions of the space and associated statistics can be calculated from the histograms. The granularity of the probability simplex must be chosen considering the size of the manifold; very small bins would generate discontinuous probability distributions that could mislead the determination of associated statistics.
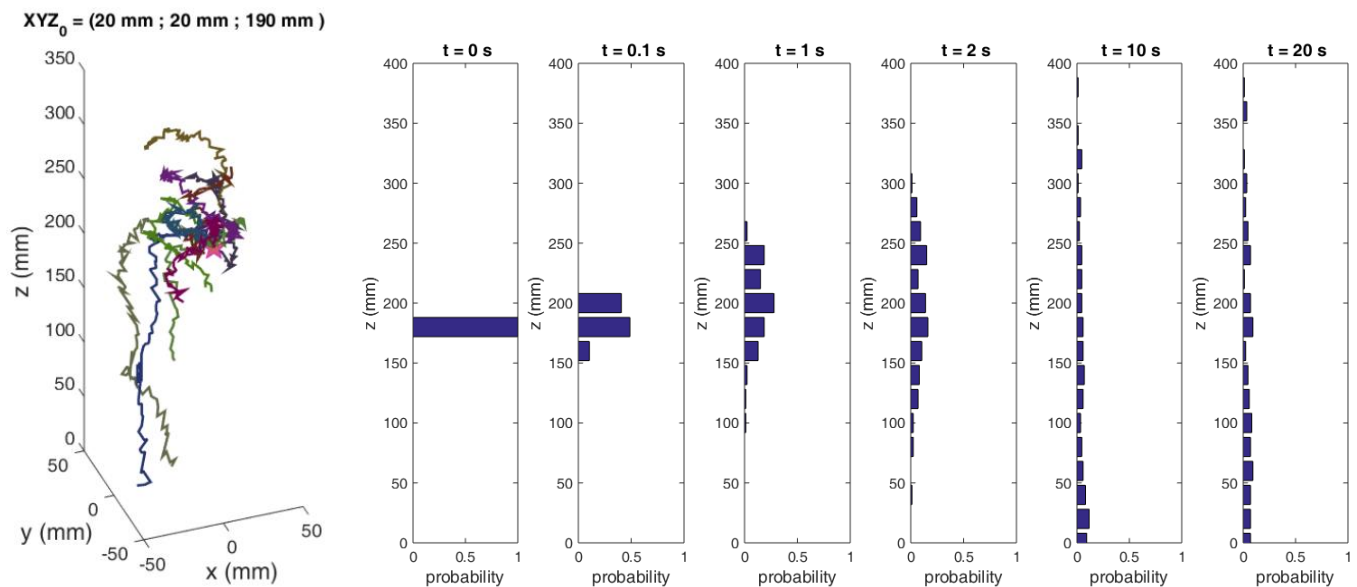

Figure 3. Manifold of three-dimensional trajectories within the GLSFB (left) and histograms (right) corresponding to the axial position at different times: 0; 0.1; 1; 2; 10 and 20 s. Axial granularity: 30.

In many cases, the distribution is not homogeneously arranged throughout the bed, especially if the traced phase differs in density with the rest of the phases of the system, e.g., solids whose density is greater than that of the fluid that disperses it. Nevertheless, there is a systematic tendency of the probability distributions to evolve to a fixed form, an

absolute convergence, dependent only on the operating conditions. After a while, these distributions do not differ from each other.

Figure 4 shows the temporal evolution of the Normalized Shannon Entropy time-series $\Omega(t)$ of a trajectory manifold starting from the same region of space. It is observed that the quantifier $\Omega(t)$ reaches an asymptotic value less than one because it is related to the distribution of the solid phase that is established once the pseudo-steady state is reached for a given operating condition. This asymptotic value corresponds to the maximum level of mixing of the phase that the tracer represents within the system. It is consistently found that Shannon's time-related path extracts have a concave curvature and converges at a precise value that depends on tracer density and gas velocity, consistent with the conception of Lyapunov dynamic equilibrium [27]. Parsimonicall chosen granularities of the probability simplex lead to the same values of asymptotic Shannon entropy.
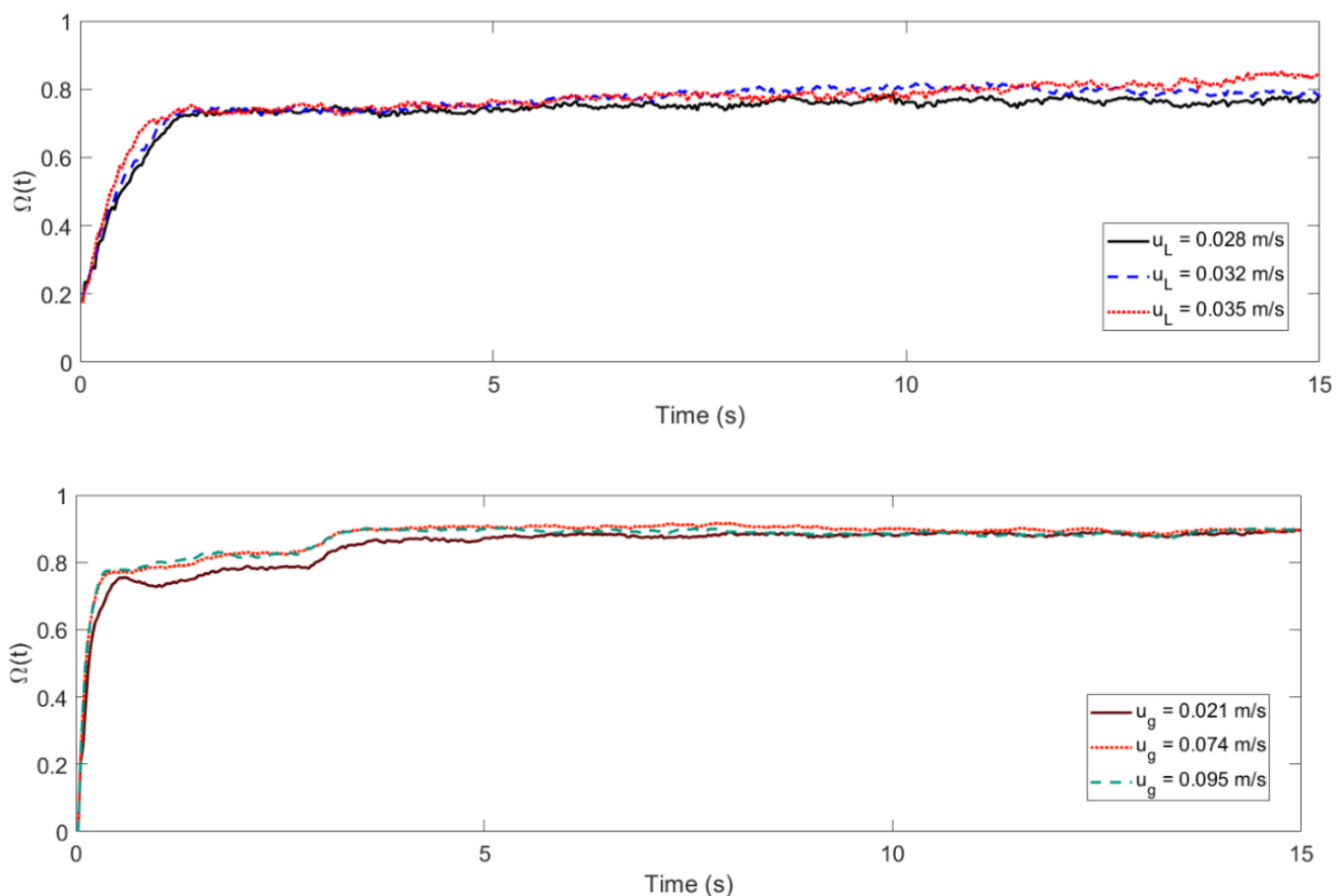

Figure 4. Normalized Shannon Entropy as a function of the manifold time for the LSFB (above) and the GLSFB (below), shown for different fluid superficial velocities.

4. - Mixing and stability assessment based on information geometry

4.1- Mixing times and Entropy Production

It is observed that, regardless of the starting point, the entropy calculated using sets of trajectory extracts reaches a quasi-invariant value in time, denoting the presence of a pseudo-stationary state. This system of suspended particles against gravity, although a

metastable state sustained by a continuous upward fluid flow, is dynamically stable in the Lyapunov sense since it reaches a constant entropy from a certain moment. Figure 5 shows the asymptotic entropy values Ω_∞ for each operative condition, determined from different starting points. Granularity values between 20 and 60 in the axial direction and 3 to 8 in the radial direction provide similar values of Ω_∞ [12], only dependent upon the operational. There is an increment of Ω_∞ values when fluid velocity increases. However, the LSFB shows a systematically lower level of mixing than those observed in the GLSFB.
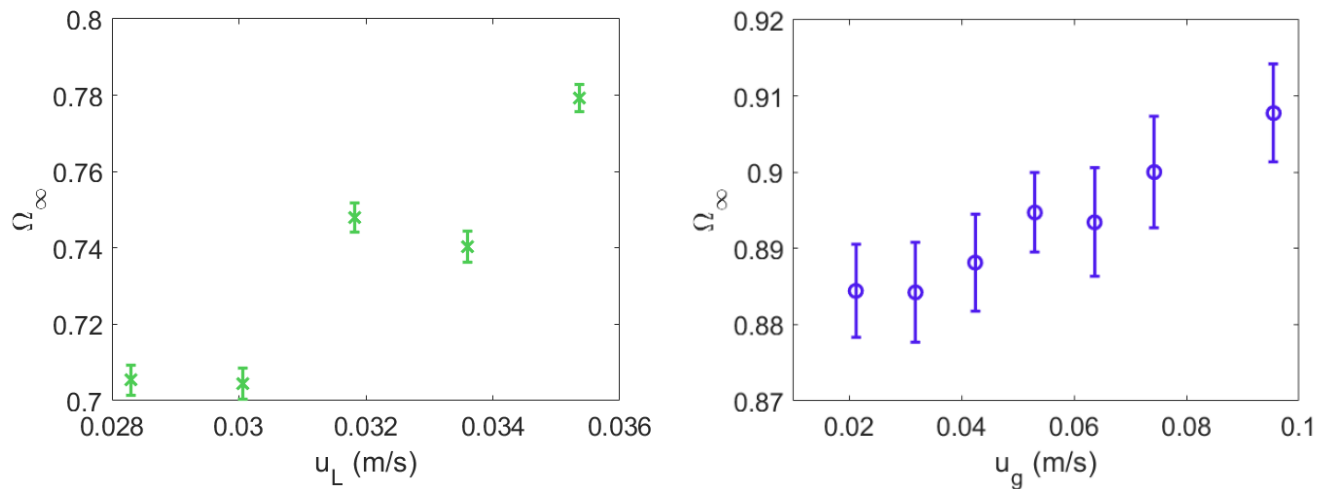

Figure 5. Asymptotical Shannon entropy as a function of the superficial fluid velocity: LSFB (left) and GLSFB (right).

The time required to reach Ω_∞ can be considered as an estimation of the mixing time. This concept is widely used to assess the dynamic thermalization of quantum systems [24]. The shape of $\Omega_{(t)}$ is usually monotonously increasing, reaching a single stationary value regardless of the 'injection point'. However, in some cases, it can temporarily reach a situation of overmixing (when the instantaneous entropy is greater than that of the steady-state). Therefore, a robust criterion to determine the mixing time is to find the first portion of the curve where the product of the slope and the regression coefficient of five subsequent points is significantly close to zero, verifying that the Ω value does not differ significantly from the plateau value [11]. Figure 6 shows the axial distribution of mixing time for different fluid velocities.

Results indicate the same order of magnitude but different axial trends for mixing times determined for the LSFB compared to the GLSFB. However, it should be recalled that the LSFB achieves a lower bed expansion and homogeneity than those observed in the GLSFB. The LSFB shows a smooth trend with a maximum of about 0.1 m. On the other hand, the GLSFB shows a sharp break at 0.15 m, and longer times are necessary to attain mixing when the manifold starts closer to the bottom [12], plausibly related to circulation patterns that trap the tracer and delay the relaxation of the probability simplex. Despite that the fluid Reynolds number is quite higher in the case of the LSFB system $\left(Re_L \in [2800; 3500]\ vs.\ Re_g \in [150; 700]\right)$, it is observed that the homogeneity levels are lower at the LSFB than those obtained in the GLSFB.
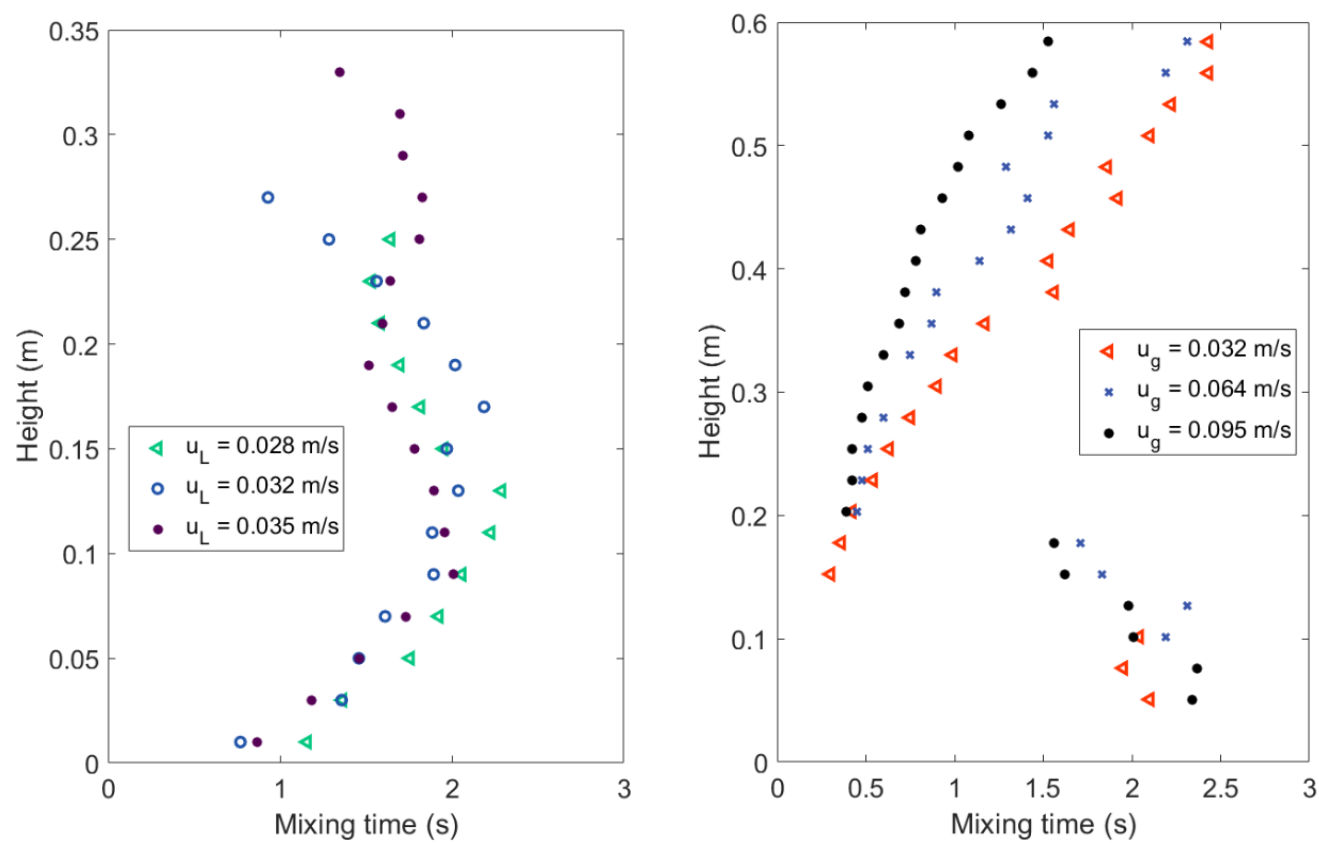
Figure 6. Axial mixing time profiles for the LSFB (left) and the GLSFB (right) systems.

Figure 7 shows the normalized entropy change reached at the macroscopic mixing time for both systems. In the GLSFB system, the highest turbulence spot is localized where the lower and upper vortices meet, naturally coinciding with the area where the mixing time is minimum. The rate of entropy production has its maximum.
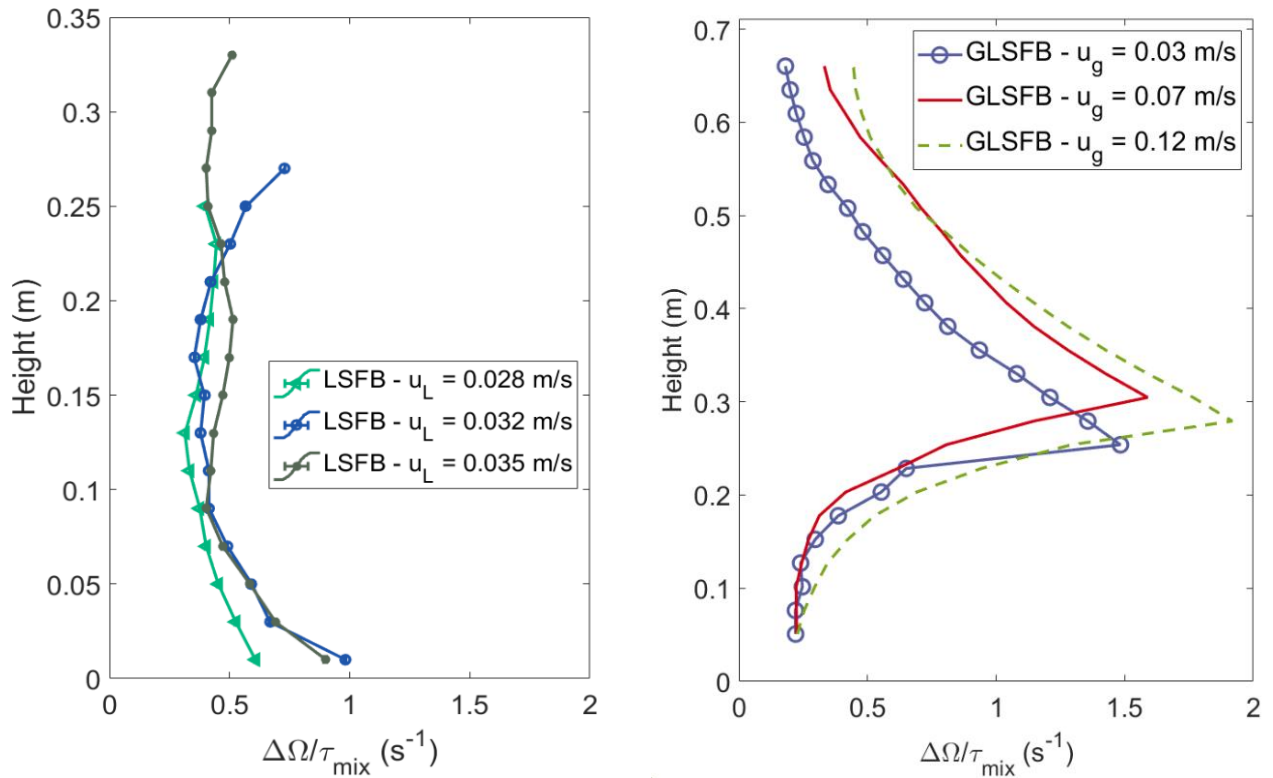
Figure 7. Normalized Shannon entropy production depending on the column height for LSFB (left) and the GLSFB (right) systems under different stirring conditions.

4.2- Glansdorff-Prigogine criterion based on the Fisher information

From the definition of the Fisher information as the squared time derivative of the Shannon entropy $(d\Omega/dt)^2$, it is feasible to obtain an approximate value from the slope of $\Omega(t)$, as shown in Figure 8. Recent theoretical investigations regarding applying information geometry to the fluctuation-response ratio of physical observables provided a general and simple criterion for stability [28–30]. According to Ito (2019), Fisher information can be interpreted as the speed change in a probability simplex evolution over time [28].
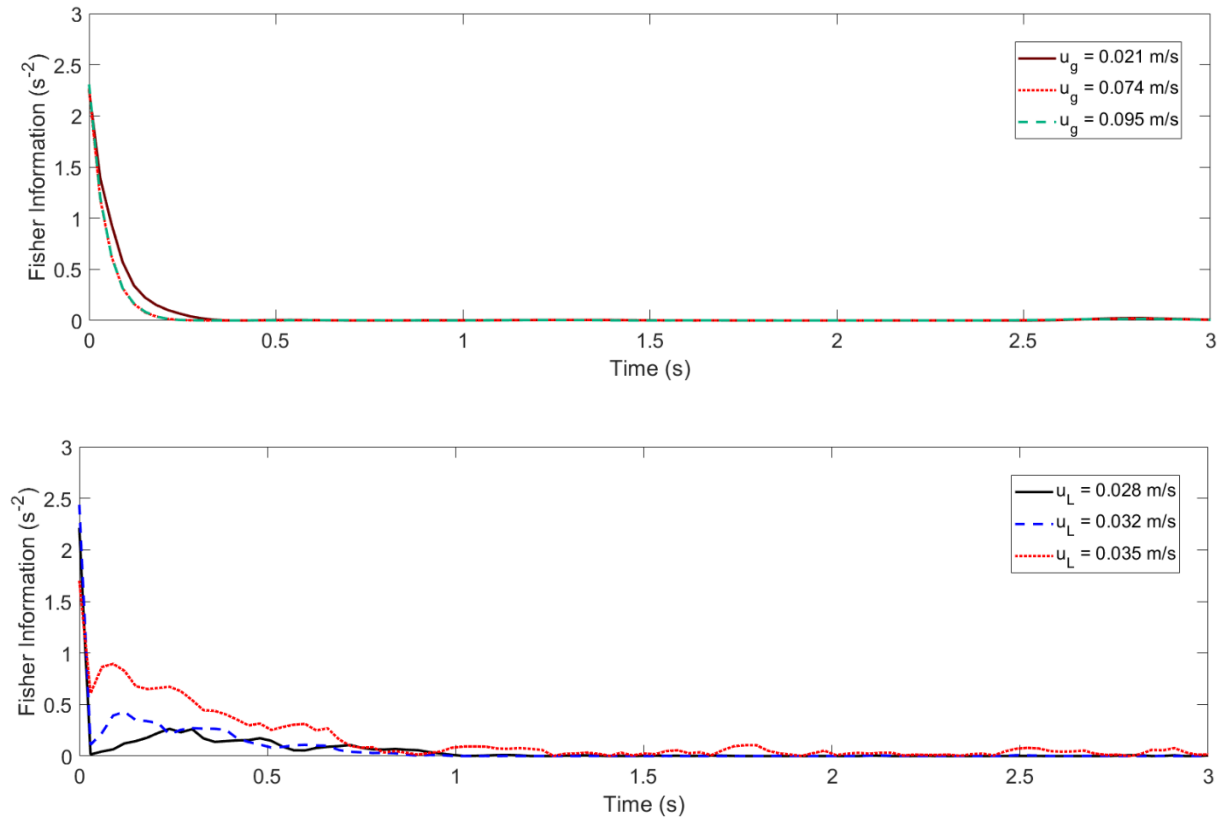
Figure 8. Fisher information as a function of time for the LSFB (above) and the GLSFB (below).

In information geometry, the fluctuation of any observable is constrained by its Fisher information. A decay of the Fisher information is equivalent to convergence to stability This criterion is the Lyapunov stability criterion with the Fisher information as the Lyapunov function [28]. The sign of the Fisher information speed rate can be used as the Glansdorff-Prigogine criterion for stability of non-stationary dynamics [28], as follows:

$$\frac{d}{dt}\left(\frac{d\Omega}{dt}\right)^2 \leq 0 \Leftrightarrow \text{Stability}$$
$$\frac{d}{dt}\left(\frac{d\Omega}{dt}\right)^2 > 0 \Leftrightarrow \text{Instability}$$

(2)

Figure 9 shows the gap values of Fisher information comparing the initial state of the manifold and the moment after mixing time. There is a clear contrast between the LSFB and the GLSFB systems; the Fisher information gap slightly increases on the LSFB operating window while the GLSFB decreases with the gas velocity. However, it is systematically checked that both fluidized systems are stable from the Glandorsff-Prigogine stability perspective.
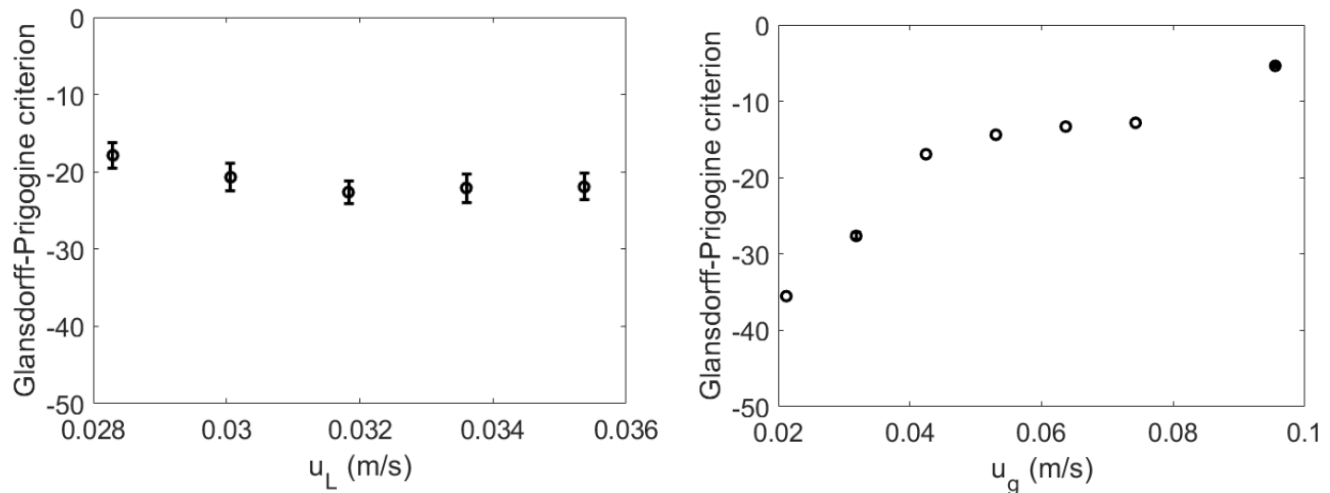
Figure 9. Fisher information variation during mixing time for the LSFB (left)
and the GLSFB (right) systems.

5- Conclusion

An advanced tomographic method that allows recovering the path of a freely moving tracer in three dimensions proved to be appropriate for extracting thorough information within multiphase systems. Radioactive Particle Tracking (RPT) data enabled the experimental stability analysis of freely moving particle trajectories within pilot-scale fluidization equipment, operated as an LSFB and a GLSFB, which are difficult to obtain otherwise. From the analysis of RPT trajectories manifolds, a normalized form of Shannon Entropy arises as a very useful statistic to study homogeneity, mixing, and stability of the fluidized particles.

Normalized Shannon entropy obtained from the trajectories determined by RPT is an excellent tool for the quantitative determination of mixing times. Axial profiles of mixing times in the GLSFB points to a sharp minimum at 0.15 m, interpreted as a hot spot of turbulence. On the other hand, the LSFB shows a smoother axial profile of mixing times. Mixing times are remarkably similar in terms of order of magnitude, pointing out that the convergence to stability is a major driver of mixing.

In all operating conditions it is observed that, regardless of the starting point, after a certain time, the entropy calculated using sets of trajectory extracts reaches, from a moment, a quasi-invariant value in time, denoting the presence of a pseudo-stationary state, indicating that the system, although it is out of equilibrium, is a thermodynamically stable system in the Lyapunov sense. In addition, new theoretical developments in information geometry confirmed a previous stability criterion based on the Shannon entropy time evolution of ensemble average manifolds. The Fisher information can be interpreted as the acceleration of the probability simplex determined from the manifold. Therefore, slowing the Fisher information means the stability of the system and vice-versa. Speed decay in the probability simplex is a necessary condition of the relaxation process. Around the stationary state, this criterion is equivalent to the Glansdorff-Prigogine criterion for stability.

Author Contributions: GS: formal analysis, writing original draft, and data visualization; AG: formal analysis, review, and editing; MM: formal analysis, data curation; JP: data visualization; MC: conceptualization, experimental design, supervision, funding acquisition; CDB: funding acquisition, review, and editing.. MAC: experimental data acquisition, review, and editing; DH: experimental data acquisition, review, and editing; HS: experimental data acquisition, editing.

Conflicts of Interest: The authors declare no conflict of interest.

References

1. Agricola, G. *De Re Metallica.*; 1556; ISBN 978-1-306-32529-5.
2. Chen, K.-H.; Wang, S.S.-S.; Show, P.-L.; Lin, G.-T.; Chang, Y.-K. A Rapid and Efficient Technique for Direct Extraction of C-Phycocyanin from Highly Turbid Spirulina Platensis Algae Using Hydrophobic Interaction Chromatography in Stirred Fluidized Bed. *Biochemical Engineering Journal* **2018**, *140*, 47–56, doi:10.1016/j.bej.2018.09.005.
3. Maciel, K.S.; Santos, L.S.; Bonomo, R.C.F.; Verissimo, L.A.A.; Minim, V.P.R.; Minim, L.A. Purification of Lactoferrin from Sweet Whey Using Ultrafiltration Followed by Expanded Bed Chromatography. *Separation and Purification Technology* **2020**, *251*, 117324, doi:10.1016/j.seppur.2020.117324.
4. Pangarkar, V.G. Process Intensification in Multiphase Reactors: From Concept to Reality. *Chemical Engineering and Processing - Process Intensification* **2017**, *120*, 1–8, doi:10.1016/j.cep.2017.06.004.
5. Van Gerven, T.; Stankiewicz, A. Structure, Energy, Synergy, Time⊙The Fundamentals of Process Intensification. *Ind. Eng. Chem. Res.* **2009**, *48*, 2465–2474, doi:10.1021/ie801501y.
6. Reay, D.; Ramshaw, C.; Harvey, A. Process Intensification. In *Process Intensification*; Elsevier, 2013; pp. 27–55 ISBN 978-0-08-098304-2.
7. Duduković, M.; Mills, P. Scale-up and Multiphase Reaction Engineering. *Current Opinion in Chemical Engineering* **2015**, *9*, 49–58, doi:10.1016/j.coche.2015.08.002.
8. Ali, N.; Al-Juwaya, T.; Al-Dahhan, M. An Advanced Evaluation of the Mechanistic Scale-up Methodology of Gas–Solid Spouted Beds Using Radioactive Particle Tracking. *Particuology* **2017**, *34*, 48–60, doi:10.1016/j.partic.2016.11.005.
9. Goniva, C.; Kloss, C.; Deen, N.G.; Kuipers, J.A.M.; Pirker, S. Influence of Rolling Friction on Single Spout Fluidized Bed Simulation. *Particuology* **2012**, *10*, 582–591, doi:10.1016/j.partic.2012.05.002.
10. Hager, A.; Kloss, C.; Goniva, C. Combining Open Source and Easy Access in the field of DEM and coupled CFD-DEM: LIGGGHTS®, CFDEM®coupling and CFDEM®workbench.

In *Computer Aided Chemical Engineering*; Friedl, A., Klemeš, J.J., Radl, S., Varbanov, P.S., Wallek, T., Eds.; 28 European Symposium on Computer Aided Process Engineering; Elsevier, 2018; Vol. 43, pp. 1699–1704.

11.   Roy, S. Radiotracer and Particle Tracking Methods, Modeling and Scale-Up. *AIChE J.* **2017**, *63*, 314–326, doi:10.1002/aic.15559.

12.   Salierno, G.; Maestri, M.; Piovano, S.; Cassanello, M.; Cardona, M.-A.; Hojman, D.; Somacal, H. Solid Motion in a Three-Phase Bubble Column Examined with Radioactive Particle Tracking. *Flow Measurement and Instrumentation* **2018**, *62*, 196–204, doi:10.1016/j.flowmeasinst.2017.10.002.

13.   Wang, M. *Industrial Tomography: Systems and Applications*; Elsevier: Boston, MA, 2015; ISBN 978-1-78242-118-4.

14.   *Non-Invasive Monitoring of Multiphase Flows*; Chaouki, J., Larachi, F., Dudukovic, M.P., Eds.; Elsevier: Amsterdam ; New York, 1997; ISBN 978-0-444-82521-6.

15.   Bhusarapu, S.; Cassanello, M.; Al-Dahhan, M.H.; Dudukovic, M.P.; Trujillo, S.; O'Hern, T.J. Dynamical Features of the Solid Motion in Gas–Solid Risers. *International Journal of Multiphase Flow* **2007**, *33*, 164–181, doi:10.1016/j.ijmultiphaseflow.2006.08.006.

16.   Salierno, G.L.; Maestri, M.; Piovano, S.; Cassanello, M.; Cardona, M.A.; Hojman, D.; Somacal, H. Discrete Axial Motion of a Radioactive Tracer Reconstructed from the Response of Axially Aligned Detectors: Application to the Analysis of a Bubble Column Dynamics. *Chemical Engineering Science* **2013**, *100*, 402–412, doi:10.1016/j.ces.2013.03.029.

17.   Shiraishi, N.; Sagawa, T. Fluctuation Theorem for Partially Masked Nonequilibrium Dynamics. *Phys. Rev. E* **2015**, *91*, 012130, doi:10.1103/PhysRevE.91.012130.

18.   Liu, M.; Liu, L.; Zhang, H.; Yi, B.; Everaert, N. Alginate Oligosaccharides Preparation, Biological Activities and Their Application in Livestock and Poultry. *Journal of Integrative Agriculture* **2021**, *20*, 24–34, doi:10.1016/S2095-3119(20)63195-1.

19.   Sutirman, Z.A.; Sanagi, M.M.; Wan Aini, W.I. Alginate-Based Adsorbents for Removal of Metal Ions and Radionuclides from Aqueous Solutions: A Review. *International Journal of Biological Macromolecules* **2021**, *174*, 216–228, doi:10.1016/j.ijbiomac.2021.01.150.

20.   Zhan, T.; Lu, S.; Liu, X.; Teng, H.; Hou, W. Alginate Derived Co3O4/Co Nanoparticles Decorated in N-Doped Porous Carbon as an Efficient Bifunctional Catalyst for Oxygen Evolution and Reduction Reactions. *Electrochimica Acta* **2018**, *265*, 681–689, doi:10.1016/j.electacta.2018.02.006.

21.   Ghorbani-Vaghei, R.; Veisi, H.; Aliani, M.H.; Mohammadi, P.; Karmakar, B. Alginate Modified Magnetic Nanoparticles to Immobilization of Gold Nanoparticles as an Efficient Magnetic Nanocatalyst for Reduction of 4-Nitrophenol in Water. *Journal of Molecular Liquids* **2021**, *327*, 114868, doi:10.1016/j.molliq.2020.114868.

22.   Salierno, G.; Maestri, M.; Piovano, S.; Cassanello, M.; Cardona, M.A.; Hojman, D.; Somacal, H. Calcium Alginate Beads Motion in a Foaming Three-Phase Bubble Column. *Chemical Engineering Journal* **2017**, *324*, 358–369, doi:10.1016/j.cej.2017.05.060.

23.   Maestri, M.; Salierno, G.; Piovano, S.; Cassanello, M.; Cardona, M.A.; Hojman, D.; Somacal, H. CFD-DEM Modeling of Solid Motion in a Water-Calcium Alginate Fluidized Column and Its Comparison with Results from Radioactive Particle Tracking. *Chemical Engineering Journal* **2019**, *377*, 120339, doi:10.1016/j.cej.2018.11.037.

24.   Shannon, C.E. A Mathematical Theory of Communication. *Bell System Technical Journal* **1948**, *27*, 379–423, doi:https://doi.org/10.1002/j.1538-7305.1948.tb01338.x.

25.   Abel, M.; Biferale, L.; Cencini, M.; Falcioni, M.; Vergni, D.; Vulpiani, A. Exit-Times and ϵ-Entropy for Dynamical Systems, Stochastic Processes, and Turbulence. *Physica D: Nonlinear Phenomena* **2000**, *147*, 12–35, doi:10.1016/S0167-2789(00)00147-0.

26.   Guida, A.; Nienow, A.W.; Barigou, M. Shannon Entropy for Local and Global Description of Mixing by Lagrangian Particle Tracking. *Chemical Engineering Science* **2010**, *65*, 2865–2883, doi:10.1016/j.ces.2009.12.041.

27.   Prigogine, I.; Nicolis, G. Self-Organisation in Nonequilibrium Systems: Towards A Dynamics of Complexity. In *Bifurcation Analysis*; Hazewinkel, M., Jurkovich, R., Paelinck, J.H.P., Eds.; Springer Netherlands: Dordrecht, 1985; pp. 3–12 ISBN 978-94-009-6241-5.

28.   Ito, S. Thermodynamics of Information Geometry as a Generalization of the Glansdorff-Prigogine Criterion for Stability. *arXiv:1908.09446 [cond-mat]* **2019**.

29.   Ito, S.; Dechant, A. Stochastic Time-Evolution, Information Geometry and the Cramer-Rao Bound. *arXiv:1810.06832 [cond-mat]* **2019**, doi:10.1103/PhysRevX.10.021056.

30.   Yoshimura, K.; Ito, S. Information Geometric Inequalities of Chemical Thermodynamics. *arXiv:2005.08444 [cond-mat, physics:physics]* **2020**.